Journal of Power Sources 243 (2013) 993–1000

Contents lists available at SciVerse ScienceDirect

Journal of Power Sources

journal homepage: www.elsevier.com/locate/jpowsour

Improving the performance of lithium–sulfur batteries by graphene coating

Xiangyang Zhou [a], Jing Xie [a], Juan Yang [a,b,*], Youlan Zou [a], Jingjing Tang [a], Songcan Wang [a], Lulu Ma [a], Qunchao Liao [a]

[a] School of Metallurgy and Environment, Central South University, Changsha 410083, China
[b] Powder Metallurgy Research Institute, Central South University, Changsha 410083, China

HIGHLIGHTS

- A novel approach for solving the capacity loss in mesoporous carbon/sulfur material.
- A hybrid structure by incorporating the merits of CMK-3 matrix and graphene skin.
- Graphene-coated mesoporous carbon/sulfur composite was synthesized.
- The RGO@CMK-3/S composite cathode exhibits improved electrochemical properties.

GRAPHICAL ABSTRACT

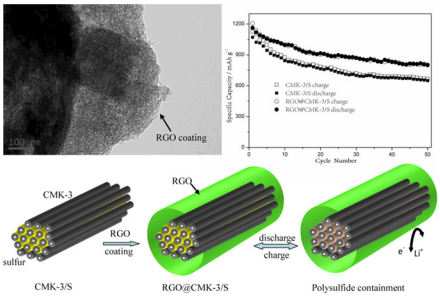

ARTICLE INFO

Article history:
Received 27 March 2013
Received in revised form
3 May 2013
Accepted 14 May 2013
Available online 19 June 2013

Keywords:
Sulfur composite
Mesoporous carbon
Graphene coating
Hybrid nanostructure
Lithium–sulfur batteries

ABSTRACT

A graphene coating mesoporous carbon/sulfur (RGO@CMK-3/S) composite, which is characteristic of a hybrid structure by incorporating the merits of CMK-3 matrix and graphene (RGO) skin, is synthesized by a facile and scalable route. The CMK-3/S composite is synthesized *via* a simple melt-diffusion strategy, and then a thin RGO skin is absorbed on the CMK-3/S composite surface in aqueous solution. When evaluating the electrochemical properties of as-prepared RGO wrapped nanostructures as cathode materials in lithium–sulfur batteries, it exhibits much improved cyclical stability and high rate performance. The RGO@CMK-3/S composite with 53.14 wt.% sulfur presents a reversible discharge capacity of about 734 mA h g^{-1} after 100 cycles at 0.5 C. The improved performance is attributed to the unique structure of RGO@CMK-3/S composite. CMK-3 with extensively mesopores can offer buffering space for the volume change of sulfur and efficient diffusion channel for lithium ions during the charge/discharge process. Meanwhile, the conductive RGO coating skin physically and chemically prevents the dissolution of polysulfides from the cathode, both of which contribute to the reduced capacity fade and improved electrochemical properties.

1. Introduction

Recently, with the rapid development of portable electronic equipment, electric vehicles and intelligent power grid and other areas, a higher demand for batteries with high power and energy density and longer cycling life has been put forward, and developing a new generation of battery system is becoming more and

* Corresponding author. School of Metallurgy and Environment, Central South University, Changsha 410083, China. Tel./fax: +86 073188836329.
E-mail address: j-yang@csu.edu.cn (J. Yang).

0378-7753/$ – see front matter © 2013 Elsevier B.V. All rights reserved.
http://dx.doi.org/10.1016/j.jpowsour.2013.05.050

more urgent [1,2]. Lithium–sulfur batteries, due to its numerous appealing characteristics such as high theoretical specific capacity (1675 mA h g^{-1}, based on the complete reactions of sulfur with lithium metal to form Li_2S), high theoretical specific energy (2500 Wh kg^{-1}, with a Li electrode), environmental benignity, abundant and cheap sulfur resources, have attracted tremendous attention and are very promising to be the next generation of high energy density lithium batteries [3–5].

However, before the full utilization of sulfur as a practical cathode material, there are still a number of issues needed to be addressed. Firstly, sulfur has a low intrinsic conductivity (5×10^{-30} S cm^{-1} at 25 °C) [4]. Secondly, the dissolution of long chain polysulfides anions (S_n^{2-}) that are generated during the charge/discharge process is the main problem [5]. Dissolved polysulfides can transfer to the lithium anode where they are reduced to form insoluble precipitates, such as Li_2S or Li_2S_2, which cause the fading of active materials. These disadvantages lead to low utilization of sulfur active material, low coulombic efficiency and rapid capacity loss during cycling [6,7]. Enormous efforts have been demonstrated to overcome the insulating property of sulfur and prevent the dissolution of polysulfides by developing novel electrolyte [8–10], embedding sulfur in nano-pores and micro-pores of active carbon [6,7,11–13], carbon nanotubes [14–17], graphene [18–21] and conductive polymer matrix [22–24]. With these strategies, the polysulfides can be trapped to some extent in the additive materials which have a large surface area and a high porous structure. Among these efforts, mesoporous carbon is a very attractive material, because of their small pore size and larger overall pore volume, incorporating sulfur into mesoporous carbon structures can contain the polysulfides to some extent during the charge/discharge process [6,11]. However, sulfur in the mesopores could still be accessed by the electrolyte in which polysulfides could be dissolved, the active material loss could only be alleviated, but not eliminated. Thus, it is essential to design novel approaches for solving the specific capacity loss caused by the dissolution of polysulfides in mesoporous carbon/sulfur composite.

Recently, several studies have shown that a high electrochemical performance nanocarbon/sulfur electrode can be achieved by designing a building block into nanocarbon/sulfur materials to form a hybrid nanostructure, such as PEG/ mesoporous carbon hybrid nanostructure [3], PEG/graphene hybrid nanostructure [19], graphene/carbon nanotubes hybrid nanostructure [25] and PEG/ carbon nanotubes hybrid nanostructure [26]. Forming hybrid structures with highly conductive carbons materials is one of the most promising methods to improve the electrochemical performance of sulfur cathodes. In addition, Graphene (or reduced graphene oxide), as a two-dimensional nanomaterial with high surface area of over 2600 m^2 g^{-1}, excellent conductivity, superior structural flexibility and mechanical strength, has been considered a viable nanocarbon component for the advanced lithium–sulfur batteries cathode electrodes [18–21,27–31]. Especially, the reduced graphene oxide which was functionalized with various groups, such as hydroxyl and carboxyl groups, could interact strongly with polysulfides to accomplish better trapping and achieve superior cycling performances [20,28]. In this work, we present a facile and scalable route to fabricate graphene-coated mesoporous carbon/sulfur composite. Active sulfur particles were highly dispersed in the channels and maintained intimate contact with the mesoporous carbon. Mesoporous carbon can offer the necessary buffering space for volume change of sulfur and efficient diffusion channel for lithium ions during the charge/discharge process as well, which acts as “micro-reactors” for the electrochemical reaction. The conductive graphene (RGO) skin coated on the surface of mesoporous carbon can trap soluble polysulfides intermediates, which can further alleviate the polysulfides shuttle [27–31]. As a result, the graphene-coated mesoporous carbon/sulfur composite shows a notably improved electrochemical performance.

2. Experimental

2.1. Material synthesis and characterization

2.1.1. Preparation of CMK-3 and CMK-3/S composite.

The CMK-3 mesoporous carbon was synthesized as described in Nazar’s paper [3]. 1.25 g glucose was dissolved in 5.0 mL of deionized water with 0.14 g H_2SO_4. 1.0 g SBA-15 (99% purity, 8 nm, 400–600 m^2/g, XF Nano, Co. Ltd, China) mesoporous silica was dispersed and sonicated in the above solution. Then the mixture was heated at 100 °C for 12 h, followed by another 12 h at 160 °C. This impregnation process was then repeated with another 5.0 ml aqueous solution containing 0.8 g glucose and 0.09 g H_2SO_4. Finally, the composite was carbonized at 900 °C for 3 h in an argon atmosphere, and SBA-15 silica template was removed by 5 wt.% HF solution at room temperature for 4 h.

The CMK-3/S composites were then prepared, in a sealed Teflon container for 12 h at 155 °C, followed by another 2 h at 300 °C under argon condition, by simply heating pre-mixed sublimed sulfur and corresponding carbon at an accurate weight ratio of 60:40. The prepared CMK-3/S composites were dispersed in 200 mL aqueous solution in which 0.2 ml of 1 wt.% Triton X-100 (a surfactant with a PEG chain) aqueous solution was added.

2.1.2. Preparation of RGO@CMK-3/S composite

Graphene oxide (GO) was synthesized by oxidation of graphite using improved Hummers’ method as reported elsewhere [32]. A certain amount of GO aqueous suspension (10.0 mg mL^{-1}) was diluted to 1.0 mg mL^{-1} with distilled water. The dispersed CMK-3/S aqueous solution was then added into the GO aqueous suspension and the mixture was sonicated for 1 h to achieve a black homogeneous aqueous suspension. A certain amount of hydrazine hydrate ($N_2H_4 \cdot H_2O$) was subsequently added to reduce graphene oxide to graphene. After stirring for 12 h at room temperature, the RGO@CMK-3/S composites were collected by consecutive centrifugation and water-washing cycles as well as lyophilization.

Characterization of CMK-3, CMK-3/S composite and RGO@CMK-3/S composite were carried out by scanning electron microscopy (SEM, JSM-6360LV, Japan), transmission electron microscopy (TEM, JEM-2100F, Japan) and X-ray diffraction (XRD, Rigaku-TTRIII, Japan).

2.2. Electrochemical measurements

The electrode consisted of 80 wt.% the as-prepared RGO@CMK-3/S composite, 10 wt.% polyvinylidene fluoride (PVDF) binder and 10 wt.% conductive carbon black. To form the sulfur electrode, the materials were mixed, dispersed in N-methyl-2-pyrrolidinone (NMP), and coated on an aluminum foil. After drying at 60 °C for 24 h, the electrodes were incorporated into 2025 coin-type cells in a glove box filled with Ar gas, using lithium metal ($\Phi = 1.54$ cm) as the counter electrode, 1 M bis(trifluoromethanesulfonyl)imide lithium (LiTFSI, Sigma–Aldrich) and 0.1 M $LiNO_3$ (Aladdin) in a mixture solution of dimethoxyethance (DME, Aldrich Co.) and 1,3-dioxolane (DOL, Aldrich Co.) (volume rate 1:1) as the electrolyte, and polyethylene film as the separator. The 2025 coin-type cells were galvanostatically cycled on a LAND CT2001A instrument (Wuhan, China) at room temperature. The cutoff potentials for charge and discharge were set at 2.8 V and 1.7 V vs. Li^+/Li, respectively. Specific capacity was corrected based on the mass of sulfur, and a typical sulfur mass loading on the electrode was 0.7-0.8 mg cm^{-2}. In this study, 1 C corresponds to a current density value of 1680 mA h g^{-1}-sulfur. Cyclic voltammograms (CV)

experiment was performed in the range of 1.6–3.0 V at a scanning rate 0.2 mV s^{-1}. Electrochemical impedance spectroscopy (EIS) measurements were performed with an impedance analyzer in the 100 kHz to 10 mHz frequency range in automatic sweep mode from high to low frequency.

3. Result and discussion

3.1. Morphologies and structures

The scanning electron microscopy (SEM) and transmission electron microscopy (TEM) analysis were used to investigate the microstructure of the as-synthesized samples. Fig. 1 a and b present the SEM images of CMK-3/S particles and RGO@CMK-3/S composite, respectively. The size of CMK-3/S particles is about 1μm. No discernible sulfur particles can be found outside of the CMK-3 particles, which suggests the full incorporation of sulfur into the channels of CMK-3. In Fig. 1b, the CMK-3/S particles are wrapped by an ultrasound, flexible and corrugated thin-film, which is the graphene sheet, indicating the feasibility of our strategy (Fig. 1g) in preparing a hybrid structure by incorporating two kinds of carbon materials. Being modified by the Triton X-100, CMK-3/S particles were well dispersed in water with hydrophilic regions. Furthermore, when GO aqueous suspension was introduced, with the aid of surface functional groups which have strong chemical interactions with sulfur [20], the GO nanosheets can self-assemble to

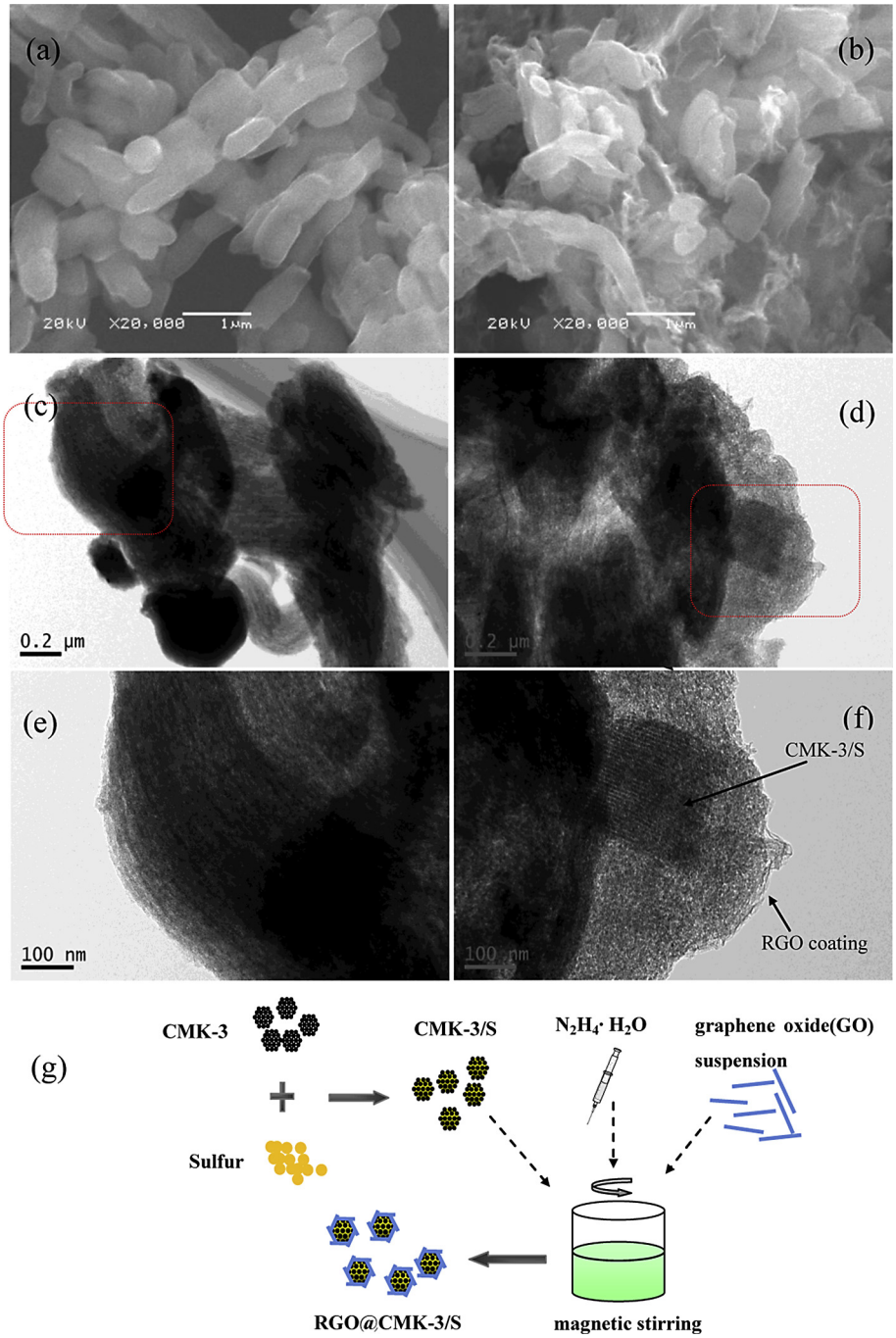

Fig. 1. SEM images of CMK-3/S composite (a) and RGO@CMK-3/S composite (b), TEM images of CMK-3/S composite (c), (e) and RGO@CMK-3/S composite (d), (f), the schematic of RGO@CKM-3/S composite preparation (g).

the surface of surfactant stabilized CMK-3/S particles, which is further confirmed by comparing the TEM images of CMK-3/S particles and RGO@CMK-3/S composite (Fig. 1 c and d). Fig. 1e and f show the zoom-in images of the region marked by the red rectangles in Fig. 1c and d, respectively. Outside the CMK-3/S particles, we can easily observe an amorphous layer tightly binding to the particles, as guided by the arrows, which is corresponding to the thin graphene film in the SEM images. Besides, vague parallel lines can also be obviously observed in the CMK-3 particles, which reflects the hexagonal packing structure of carbon tubes in the CMK-3 mesoporous carbon [2]. Undoubtedly, this hybrid structural feature can not only greatly bind CMK-3/S particles closer, but also effectively decrease or avoid the electrical disconnection between the CMK-3 clusters created by the surface deposition of insulating sulfur and its reaction products.

To further understand the composition and structure of the RGO@CMK-3/S composite, X-ray diffraction (XRD) is used, as exhibited in the Fig. 2. Fig. 2a and b show the characteristic XRD pattern of the simple mixture of CMK-3/sulfur powder and the as-prepared CMK-3 particles, respectively. Compared with the pattern of the simple mixture of CMK-3/sulfur powder, the characteristic sulfur peaks in the XRD pattern of CMK-3/sulfur composite and RGO@CMK-3/S composite are not easily detectable. This result indicates that sulfur becomes amorphous and homogeneously distributed in the CMK-3 carbon matrix [3], which agrees well with the result of the SEM and TEM images.

As shown in Fig. 3, thermogravimetric analysis (TGA) was carried out to measure the accurate sulfur content in the CMK-3/S composite and the RGO@CMK-3/S composite. The TGA curve depicts weight losses of the composite correlated to the sublimation of sulfur under N_2 atmosphere, and the sulfur content in the CMK-3/S composite and the RGO@CMK-3/S composite is 59.27 wt.% and 53.14 wt.%, respectively. According to the insolubilization of the CMK-3/S composite in the aqueous solution, we can calculate the RGO content in the RGO@CMK-3/S composite, which is about 10 wt.%. In addition, compared with some carbon/sulfur composites [7,11], the sulfur component in the composite evaporates at a much higher temperature, which suggests that the RGO@CMK-3/S composite has a nice encapsulation capability [33].

3.2. Charge/discharge curves and cycling performance

In order to demonstrate the advantageous electrochemical properties of the RGO@CMK-3/S composite, CMK-3/S composite

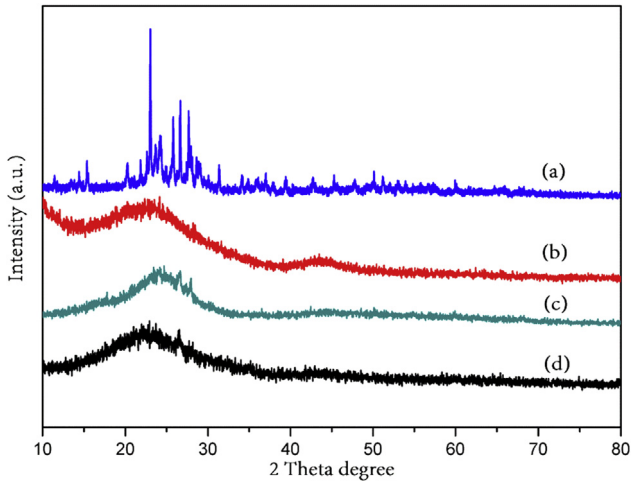

Fig. 2. The XRD patterns of (a) the simple mixture of CMK-3/sulfur powder, (b) CMK-3, (c) CMK-3/S composite and (d) RGO@CMK-3/S composite.

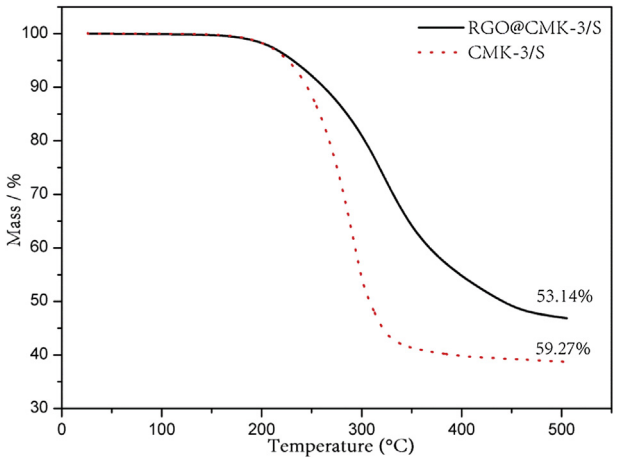

Fig. 3. TG curves recorded for CMK-3/S composite and RGO@CMK-3/S composite under nitrogen flow.

with 53 wt.% sulfur were prepared by the same melt-diffusion strategy for comparison. Fig. 4a and b display the initial discharge/charge curves at different discharge rate of the lithium–sulfur batteries with the CMK-3/S and RGO@CMK-3/S cathodes, respectively. Both discharge profiles have two-voltage plateaus: the higher one at 2.4–2.2 V and the predominantly lower one at 2.1–1.8 V. These two discharge plateaus match very well with two cathodic peaks in the CV curves (as shown in Fig. 5 a). However, there exist obvious differences between the two discharge plateaus. The first discharge plateau is relatively shorter, while the second one extends longer and contributes to the majority of the discharge capacity [34]. The second discharge stages present a long horizontal plateau, which implies a highly complete reduction process from polysulfides to sulfides [35]. These voltage profiles demonstrate that the discharge capacity of the RGO@CMK-3/S cathode is higher than those of the CMK-3/S cathode at the same discharge rate. Especially, when discharge/charge rate increases, for the RGO@CMK-3/S composite cathode, a high initial specific capacity of up to 1147.7 mA h g^{-1} at 0.5 C was obtained which is about 68.3% of the theoretical capacity of sulfur. This means that at less 1.37 electrons were involved in the electrochemical reactions of the RGO@CMK-3/S cathode. However, the initial specific capacity of the CMK-3/S composite is 856.3 mA h g^{-1} at 0.5 C, corresponding to 51.0% of the theoretical capacity of sulfur, which means that only 1.02 electrons were involved in the electrochemical reactions of the CMK-3/S cathode. Such high specific capacity is due to the highly conductive RGO coating skin, which can provide a fast electron transport in the designed hybrid structure, leading to a high accessibility of active sulfur.

Fig. 5 a shows the typical cyclic voltammetry (CV) curves of the RGO@CMK-3/S composite electrode in the voltage range of 1.6–3.0 V with a constant scan rate of 0.2 mV s^{-1}. As seen, there are two peaks in the reduction process of RGO@CMK-3/S composite. The upper plateau at ~2.25 V involves the reduction of elemental sulfur to lithium polysulfides (Li_2S_n, $4 \leq n < 8$), and the lower plateau at ~2.0 V corresponds to the reduction of sulfur in lithium polysulfides to Li_2S_2 and eventually to Li_2S [36]. Two partially overlapping oxidation peaks at 2.3–2.4 V and 2.4–2.5 V are associated with the reversible conversion of Li_2S_2/Li_2S to low-order polysulfides and then to high-order polysulfides, respectively [37]. In contrast to the only one anodic peak at 2.4 V reported in other literatures [6,7,36], the two separated oxidation peaks with somewhat overlapping features imply staged reversible transitions between Li_2S_2/Li_2S and high-order polysulfides during the charging process [37].

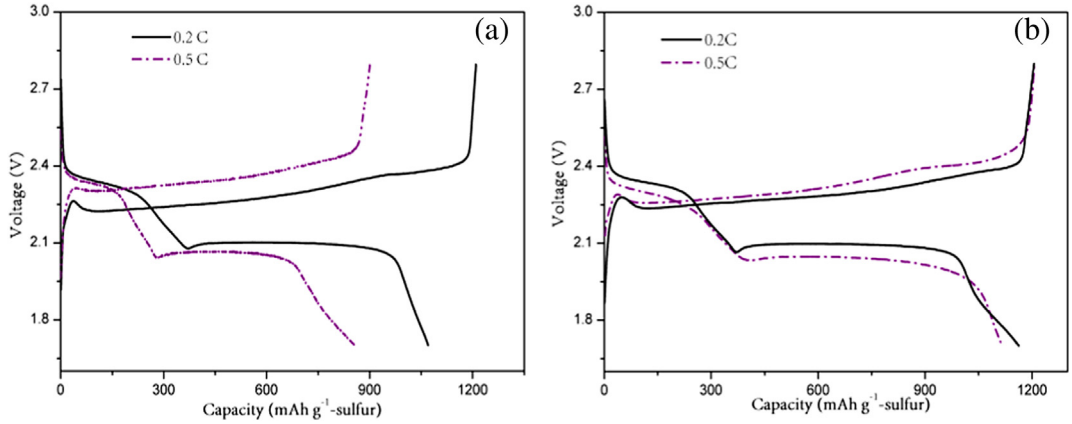

Fig. 4. The initial discharge/charge curves at 0.2 C and 0.5 C rate of the lithium–sulfur batteries with (a) CMK-3/S cathode and (b) RGO@CMK-3/S cathode.

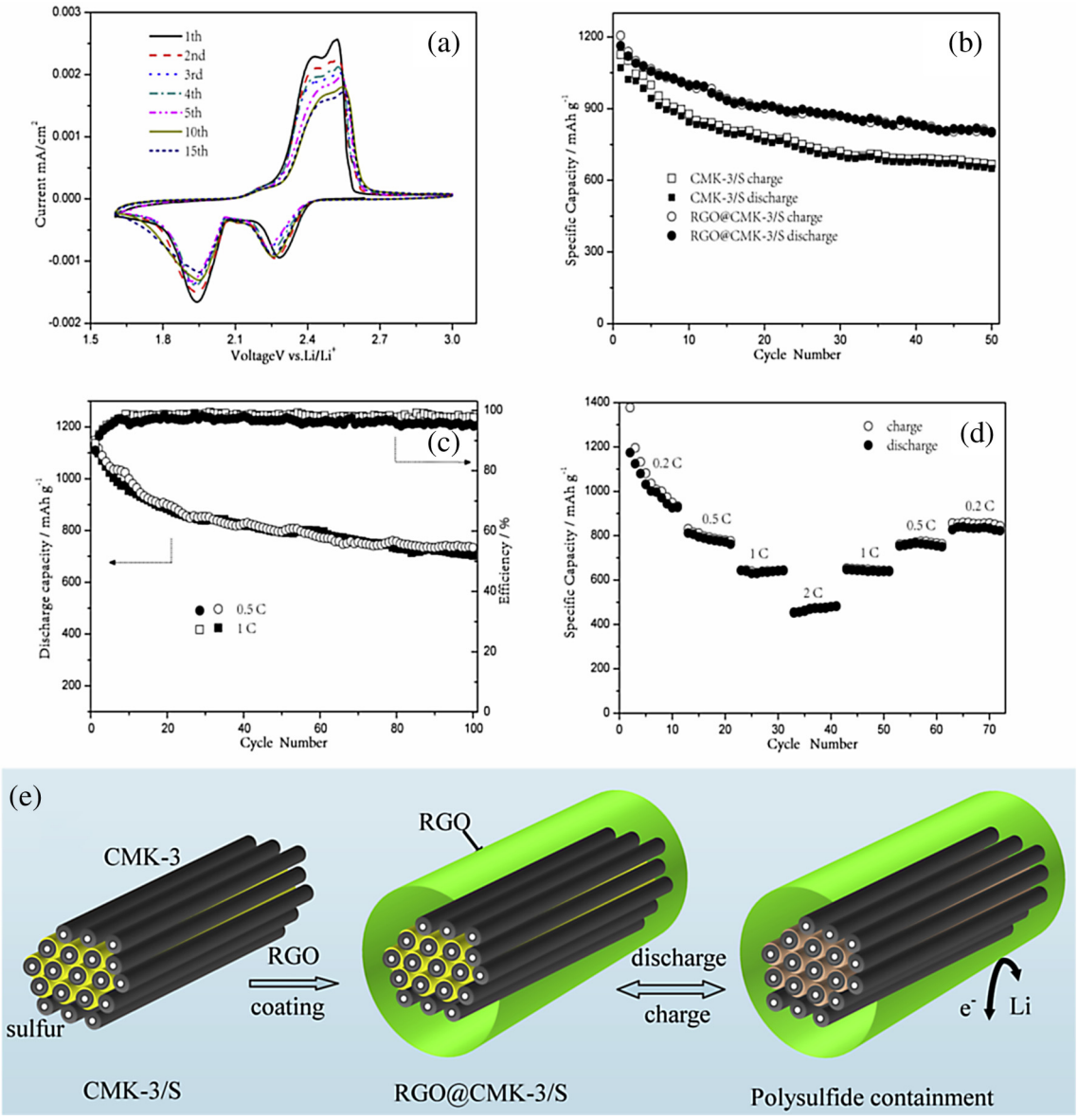

Fig. 5. (a) Cyclic voltammograms of the RGO@CMK-3/S cathode in the potential window from 1.6 to 3.0 V (versus Li/Li$^+$) at the scan rate of 0.2 mV s^{-1}, (b) cycling performances of RGO@CMK-3/S composite and CMK-3/S composite at 0.2 C, (c) cycling performances of RGO@CMK-3/S composite at 0.5 C and 1 C, (d) rate capability of RGO@CMK-3/S composite, (e) scheme of RGO@CMK-3/S composite for improving the cathode performance.

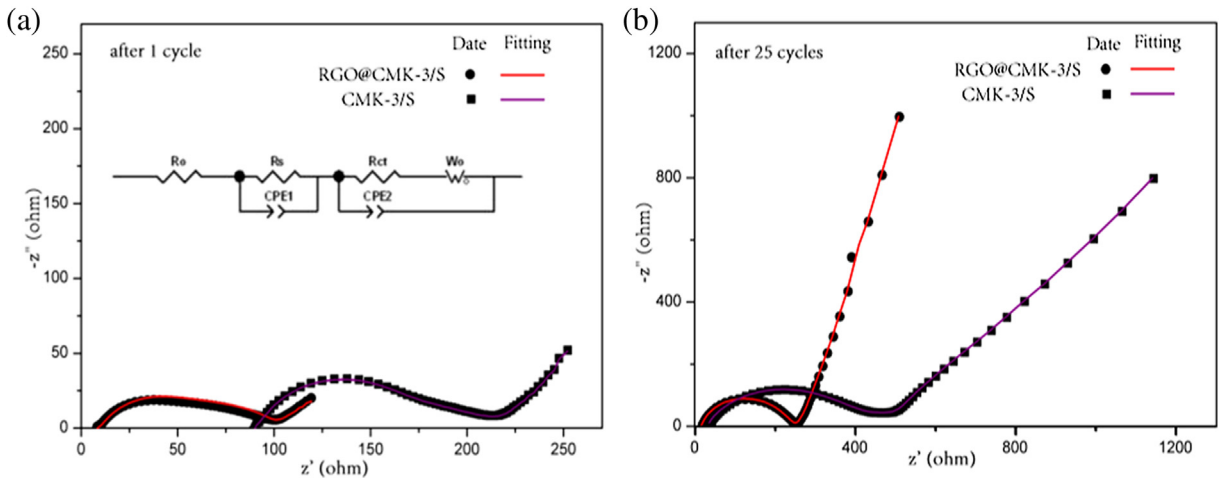

Fig. 6. EIS data for the lithium–sulfur half cell with RGO@CMK-3/S composite and CMK-3/S composite as cathode between 0.01 and 10^5 Hz.

These attractive physicochemical characteristics of the RGO@CMK-3/S composite are directly reflected in its cyclic performance and rate-capacity. Fig. 5b compares the cycling stability of RGO@CMK-3/S and CMK-3/S composite at 0.2 C, the RGO@CMK-3/S composite exhibits better cycling durability than CMK-3/S composite. After 50 cycles, the RGO@CMK-3/S composite electrode retains a capacity of 800 mA h g^{-1} *vs.* 1162 mA h g^{-1} at first cycle. While the discharge capacity of the CMK-3/S composite shows lower specific capacity and only 649.2 mA h g^{-1} could be delivered after 50 cycles *vs.* 1070.6 mA h g^{-1} at the first cycle. Although the sulfur cathode is known to suffer from sluggish kinetics, our RGO@CMK-3/S composite electrode demonstrated high specific capacities and cycling stabilities when cycled at higher rates, as shown in Fig. 5c. At a rate of 0.5 C and 1 C, the RGO@CMK-3/S composite cathode delivered high initial specific capacity of 1147.7 mA h g^{-1} and 1134.7 mA h g^{-1}, respectively. After 100 cycles, the specific capacity still remains 734 mA h g^{-1} and 703 mA h g^{-1}, with an average coulombic efficiency of 95% and 98% respectively. Meanwhile, the rate capacity of cell with RGO@CMK-3/S composite cathode is shown in the Fig. 5d. During the first ten cycles, the discharge capacity faded gradually at 0.2 C rate. However, when the cell operated at 0.5C, 1C and 2C rate, the RGO@CMK-3/S composite electrode delivered a capacity of 770 mA h g^{-1}, 642 mA h g^{-1} and 482 mA h g^{-1}, respectively. And then the rate was reset back to 1C, 0.5C and 0.2C, the electrode resumes the capacity of 640 mA h g^{-1}, 750 mA h g^{-1} and 835 mA h g^{-1}, respectively, without abrupt capacity fade. The result indicates good robustness and stability of the cathode material.

This outstanding cyclability can be understood through the specific microstructure of RGO@CMK-3/S (Fig. 5e). First, due to an extremely high surface area and high pore volume of CMK-3, active sulfur particles were highly dispersed in the channels and maintained intimate contact with the CMK-3. CMK-3 can offer the necessary buffering space for the volume change of sulfur and efficient diffusion channel for lithium ions during the charge/discharge process, which acts as "micro-reactors" for the electrochemical reaction. Second, both the CMK-3 and RGO coating layers have excellent adsorption properties. Importantly, the conductive graphene (RGO) skin coated on the surface of CMK-3, which contains the residual oxygen-containing functional groups, could implant chemical and physical barriers in cathode for adsorbing polysulphides anions [27–31], thus minimizing the shuttle reaction and mass loss of the active materials during cycles. Consequently, the RGO@CMK-3/S composite exhibits an outstanding rate capability and improved cycling performance. However, as some capacity loss still occurred during the cycling process, the problem of polysulfides dissolution has not been solved completely. Because there may be some layer gaps in the thin graphene film, a small amount of polysulfides formed during charge/discharge process can still diffuse out of the RGO@CMK-3/S particles and initiate the capacity loss.

3.3. Electrochemical impedance spectra

To understand the improved electrochemical performance after coating RGO skin on the CMK-3/S composite, the electrochemical impedance spectroscopy (EIS) was measured for the CMK-3/S composite and RGO@CMK-3/S composite electrodes after the 1st and 25th cycle, respectively. As shown in Fig. 6, all of the impedance spectra have similar feature: a medium-to-high frequency depressed semi-circle and an inclined low-frequency line. The intercept at real axis Z' corresponds to the combination resistance R_o, which represents the ionic resistance of the electrolyte, the contact resistance at the active material/current collector interface and the intrinsic resistance of the active materials. The semicircle in the high-frequency region corresponds to Li^+ migration through the SEI films (R_s), and the medium frequency region relates to charge transfer resistance (R_{ct}). The inclined line at the low-frequency region corresponds to the Warburg impedance (W), which is associated with Li^+ diffusion in the electrode. [30,38–40]

In order to understand those phenomena better, a relevant equivalent circuit model was incorporated to fit the data points. It can be seen from the Fig. 6a, the Nyquist plots were fitted by an equivalent circuit composed of R_o in series to a parallel circuit element that branches into R_s and constant phase element (CPE1), followed by another parallel circuit element that branches into R_{ct} with W and the constant phase element (CPE2). Table 1 shows electrode resistance obtained from the equivalent circuit fitting of

Table 1
Electrode resistance obtained from the equivalent circuit fitting of experimental data.

Sample	Cycle	R_o (Ω)	R_s (Ω)	R_{ct} (Ω)
CMK-3/S	1	91.5	70.35	42.37
	25	31.64	293.2	154.2
RGO@CMK-3/S	1	17.08	44.72	54.37
	25	16.22	170.9	53.1

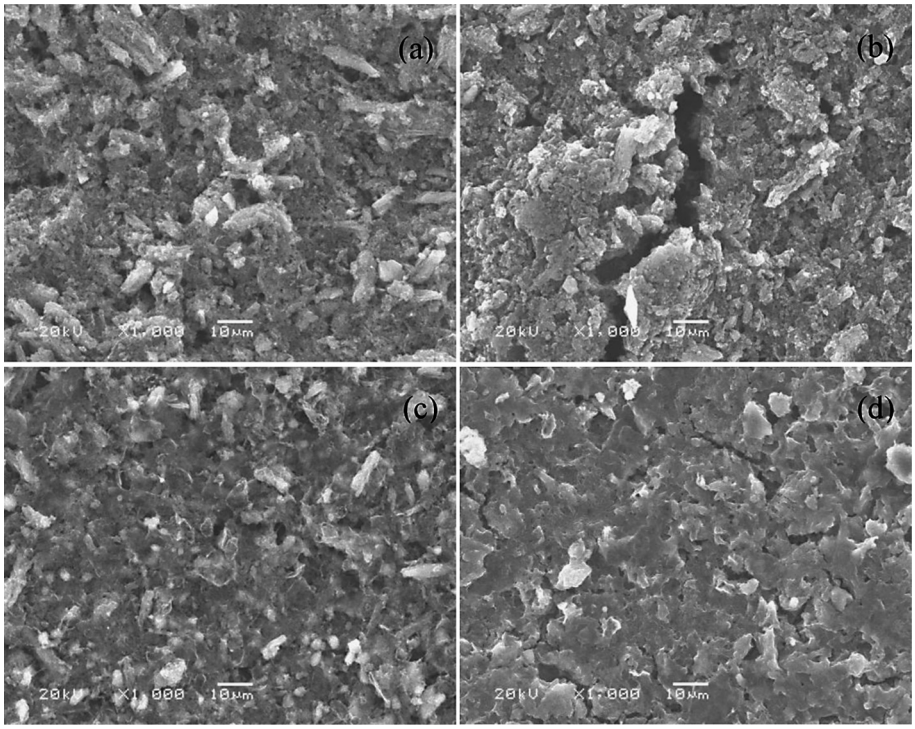

Fig. 7. SEM images of cathode (a) the as-prepared CMK-3/S composite cathode, (b) the CMK-3/S composite cathode after 25 cycles, (c) the as-prepared RGO@CMK-3/S composite cathode, (d) the RGO@CMK-3/S composite cathode after 25 cycles.

experimental data. R_o of the RGO@CMK-3/S composite electrode after 1 cycle (17.08 Ω) and after 25 cycles (16.22 Ω) were much lower than the CMK-3/S composite electrode before (91.5 Ω) and after 25 cycles (31.64 Ω), respectively. It demonstrates that the intrinsic resistance of RGO@CMK-3/S composite is lower than the CMK-3/S composite, probably due to the excellent conductivity of the RGO skin. After 25 cycles, R_s of the two cathodes increased similarly, which maybe relate to the further corrosion of lithium in the electrolyte. Comparatively, the charge transfer resistance R_{ct} of CMK-3/S composite significantly increased as the cell cycled to 25th, which results from the irreversible deposition and aggregation of insulated Li_2S_2/Li_2S on the CMK-3 surface. However, R_{ct} of the RGO@CMK-3/S composite remained the same. This is probably due to the hybrid structure of the RGO@CMK-3/S composite, which is in favor of the rapid electronic/ionic transport and meanwhile can trap soluble polysulfides intermediates inside the composite particles. Furthermore, the hybrid structure could act as a continuous 3D network, which could provide efficient accessibility of active material to the electrolyte. The EIS results also explain why the RGO@CMK-3/S composite displays an improved electrochemical performance.

3.4. Morphologies of sulfur cathode

The as prepared cathode samples after 25 cycles were washed with DMC (Dimethyl carbonate) in an argon-filled glove box. After drying at ambient temperature for 24 h in the glove box, the samples were transferred to the SEM system immediately. Fig. 7 shows the SEM images of CMK-3/S electrode and RGO@CMK-3/S electrode before cycle and after 25 cycles. It can be seen from Fig. 7a and c that the CMK-3/S and RGO@CMK-3/S composite are both highly dispersed in the electrode before cycles. However, after 25 cycles, A significant structural damage occurred in the CMK-3/S electrode (Fig. 7 b). It seems that part of sulfur in the CMK-3 could be accessed directly by electrolyte in which polysulfides could be dissolved due to limited adsorption abilities of CMK-3, and casually deposited on the surface of the electrode during the cycles. In contrast, the RGO@CMK-3/S electrode retained its own structure well and displayed a homogeneous distribution of the RGO@CMK-3/S materials as shown in Fig. 7 b and d, which may be explained from the unique structure of RGO@CMK-3/S composite. Owing to its porous structure, CMK-3 could provide a certain internal void space to accommodate the volume expansion of sulfur during the discharge process. In addition, the RGO coating on the CMK-3/S particles could provide a flexible cushion in the RGO@CMK-3/S composite to maintain the CMK-3/S particles' shape without being destroyed even when the CMK-3 particles could not hold the volume expansion of sulfur. Thus, the collapse of the microarchitecture of the electrode can be prevented and undesirable capacity loss by their dissolution during the cycles.

4. Conclusions

In this paper, graphene-coated mesoporous carbon/sulfur composite was successfully synthesized. It has been demonstrated that the mesoporous carbon sphere (CMK-3) with unique channel can highly ensure a good electrical path for the active sulfur, and conductive graphene (RGO) skin coated on the surface of mesoporous carbon can trap soluble polysulfides intermediates effectively and minimize the loss of active mass in cathode, which leads to a notable improvement of electrochemical performance of lithium–sulfur batteries. A reversible discharge capacity of about 734 mA h g^{-1} after 100 cycles at 0.5 C was obtained, which is higher than that of the counterpart without graphene coating. Moreover, the RGO@CMK-3/S composite manifests an outstanding rate capability. The strategy of developing a hybrid structure by

incorporating the merits of CMK-3 matrix and graphene (RGO) skin, has great advantages, and can be a feasible way to improve the performance of other electrode materials in lithium ion batteries.

Acknowledgments

This study was supported by the National Natural Science Foundation of China (51274240 and 51204209).

References

[1] X. Ji, L.F. Nazar, J. Mater. Chem. 20 (2010) 9821–9826.
[2] Y. Yang, G.H. Yu, J.J. Cha, H. Wu, M. Vosgueritchian, Y. Yao, Z.N. Bao, Y. Cui, ACS Nano 5 (2011) 9187–9193.
[3] X. Ji, K.T. Lee, L.F. Nazar, Nat. Mater. 8 (2009) 500.
[4] L.C. Yin, J.L. W, F.J. Lin, J. Yang, Y.N. Nuli, Energy Environ. Sci. 5 (2012) 6966–6972.
[5] J. Nelson, S. Misra, Y. Yang, A. Jackson, Y. Liu, H. Wang, H. Dai, J.C. Andrews, Y. Cui, M.F. Toney, J. Am. Chem. Soc. 134 (2012) 6337–6343.
[6] X. Liang, Z.Y. Wen, Y. Liu, H. Zhang, L.Z. Huang, J. Jin, J. Power Sources 196 (2011) 3655–3658.
[7] S.R. Chen, Y.P. Zhai, G.L. Xu, Y.X. Jiang, D.Y. Zhao, J.T. Li, L. Huang, S.G. Sun, Electrochem. Acta 56 (2011) 9549–9555.
[8] J.H. Shin, E.J. Cairns, J. Power Sources 177 (2008) 537–545.
[9] M. Nagao, A. Hayashi, M. Tatsumisago, Electrochem. Acta 56 (2011) 6055–6059.
[10] S. Zhang, Electrochem. Acta 70 (2012) 344–348.
[11] G. He, X.L. Ji, L. Nazar, Energy Environ. Sci. 4 (2011) 2878.
[12] D.W. Wang, G.M. Zhou, F.L.K.H. Wu, G.Q. Lu, H.M. Cheng, L.R. Gentle, Phy. Chem. Chem. Phys. 14 (2012) 8703–8710.
[13] J. Wang, S.Y. Chew, Z.W. Zhao, S. Ashraf, D. Wexler, J. Chen, S.H. Ng, S.L. Chou, H.K. Liu, Carbon 46 (2008) 229–235.
[14] J.J. Chen, Q. Zhang, Y.N. Shi, L.L. Qin, Y. Cao, M.S. Zheng, Q.F. Dong, Phys. Chem. Chem. Phys. 14 (2012) 5376–5382.
[15] L.X. Yuan, H.P. Yuan, X.P. Qiu, L.Q. Chen, W.T. Zhu, J. Power Sources 189 (2009) 1141–1146.
[16] J.C. Guo, Y.H.X.C.H. Wang, Nano Lett. 11 (2011) 4288–4294.
[17] W. Wei, J.L. Wang, L.J. Zhou, J. Yang, B. Schumann, Y. NuLi, Electrochem. Commun. 13 (2011) 399–402.
[18] N. Li, M. Zheng, H. Lu, Z. Hu, C. Shen, X. Chang, G. Ji, J. Cao, Y. Shi, Chem. Commun. 48 (2012) 4106–4108.
[19] H. Wang, Y. Yang, Y. Liang, J.T. Robinson, Y. Li, A. Jackson, Y. Cui, H. Dai, Nano Lett. 11 (2011) 2644–2647.
[20] L.W. Ji, M.M. Rao, H.M. Zheng, L. Zhang, Yu. C. Li, W.H. Duan, J.H. Guo, E.J. Cairns, Y.G. Zhang, J. Am. Chem. Soc. 133 (2011) 18522–18525.
[21] S. Evers, L.F. Nazar, Chem. Commun. 48 (2012) 1233–1235.
[22] Y.Z. Fu, A. Manthiram, RSC Advances 2 (2012) 5927–5929.
[23] F. Wu, J.Z. Chen, R.J. Chen, S.X. Wu, L. Li, S. Chen, T. Zhao, J. Phys. Chem. C 115 (2011) 6057–6063.
[24] G.C. Li, G.R. Li, S.H. Ye, X.P. Gao, Adv. Energy Mater. 2 (2012) 1238–1245.
[25] M. Zhao, X. Liu, Q. Zhang, G. Tian, J. Huang, W. Zhu, F. Wei, ACS NANO 6 (2012) 10759–10769.
[26] S. Zhang, Q. Zhang, J. Huang, X. Liu, W. Zhu, M. Zhao, W. Qian, F. Wei, Part. Part. Syst. Charact. 30 (2013) 158–165.
[27] J.Z. Wang, L. Lu, M. Choucair, J.A. Stride, X. Xu, H. Liu, J. Power Sources 196 (2011) 7030–7034.
[28] H. Sun, G. Xu, Y. Xu, S. Sun, X. Zhang, Y. Qiu, S. Yang, Nano Res. 5 (2012) 726–738.
[29] J. Huang, X. Liu, Q. Zhang, C. Chen, M. Zhao, S. Zhang, W. Zhu, W. Qian, W.F. Wei, Nano Energy 2 (2013) 314–321.
[30] X. He, L. Wang, J. Li, J. Gao, M. Fang, G. Tian, J. Wang, S. Fan, J. Power Sources, http://dx.doi.org/10.1016/j.jpowsour.2013.02.008.
[31] B. Wang, K. Li, D. Su, H. Ahn, G. Wang, CHEM-ASIAN J 7 (2012) 1637–1643.
[32] L.L. Zhang, S.Y. Zhao, X.N. Tian, X.S. Zhao, Langmuir 26 (2010) 17624–17628.
[33] B. Ding, C.Z. Yuan, L.F. Shen, G.Y. Xu, P. Nie, X.G. Zhang, Chem. Eur. J. 19 (2013) 1013–1019.
[34] K.F. Li, B. Wang, D.W. Su, J. Park, H. Ahn, G.X. Wang, J. Power Sources 202 (2012) 389–393.
[35] E. Peled, A. Gorenshtein, M. Segal, Y. Sternberg, J. Power Sources 26 (1989) 269–271.
[36] C.F. Zhang, H.B. Wu, C.Z. Yuan, Z.P. Guo, X.W. David Lou, Angew. Chem. Int. Ed. 51 (2012) 9592–9595.
[37] Y. Fu, A. Manthiram, J. Phys. Chem. C 116 (2012) 8910–8915.
[38] B. Ding, C. Yuan, L. Shen, G. Xu, P. Nie, Q. Lai, X.G. Zhang, J. Mater. Chem. A 1 (2013) 1096–1101.
[39] M. Rao, X.Y. Song, E.J. Cairns, J. Power Sources 205 (2012) 474–478.
[40] Y. Wang, L. Huang, L. Sun, S. Xie, G. Xu, S. Chen, Y. Xu, J. Li, S. Chou, S. Dou, S. Sun, J. Mater. Chem. 22 (2012) 4744–4750.